Sensors and Materials, Vol. 38, No. 1 (2026) 1–12
MYU Tokyo

S & M 4280

Additive Manufacturing of High-performance Sandwich-type Flexible Strain Sensors Based on MWCNT–graphene/TPU Composites

Deqiao Xie,[1*] Fuxi Liu,[2**] and Fei Lv[3]

[1]College of Astronautics, Nanjing University of Aeronautics and Astronautics, Nanjing 210016, China
[2]Beijing Xinghang Electric-Mechanical Equipment Co., Ltd., Beijing 100071, China
[3]Laboratory of High Power Fiber Laser Technology, Shanghai Institute of Optics and Fine Mechanics, Chinese Academy of Sciences, Shanghai, 201800, China

(Received August 18, 2025; accepted November 11, 2025)

Keywords: additive manufacturing, photocuring, flexible sensor, sandwich structure, MWCNT–graphene/TPU composites

The rapid development of flexible electronics has led to an increasing demand for multifunctional flexible sensors. However, the preparation of such sensors is still limited by material and equipment constraints. The aim of this study is to develop a novel method for fabricating high-performance sandwich-type flexible strain sensors using photocuring additive manufacturing technology to address the limitations of current fabrication methods. A flexible conductive composite resin was prepared by the simple mixing of materials. A custom multimaterial digital light processing (DLP) system was used to integrate multiple materials and form the sandwich structure. The mechanical and electrical properties of the resulting sensor were evaluated through a series of experiments. The sensor exhibited a high sensitivity coefficient of 5.355, an impressive deformation capability of up to 105%, and excellent mechanical durability. The strong adhesion between layers and the enhanced mechanical properties of the sandwich structure contributed to its superior performance compared with single-material sensors. Additionally, the sensor was successfully applied to monitor the flight motion of a flapping-wing aircraft, demonstrating its potential for practical applications. This work provides a simplified and efficient method for fabricating flexible sensors and valuable insights for the development of next-generation wearable and flexible electronic devices.

1. Introduction

Compared with traditional rigid strain sensors, flexible strain sensors have higher flexibility, ductility, and biocompatibility, and thus hold great potential in human-computer interaction and medical monitoring in modern society.(1) Flexible sensors that exhibit force-induced resistance changes under strain have garnered extensive research attention owing to their superior tensile

*Corresponding author: e-mail: dqxie@nuaa.edu.cn
**Corresponding author: e-mail: liufx@nuaa.edu.cn
https://doi.org/10.18494/SAM5881

ISSN 0914-4935
https://myukk.org/

properties and high sensitivity coefficients. These strain sensors are typically fabricated by incorporating conductive fillers into flexible matrices.[2] Common conductive fillers include carbon black,[3] carbon nanotubes,[4],graphene,[5] and silver nanowires,[6] while common flexible polymer substrates mainly consist of silicone rubber (SR),[7] thermoplastic polyurethane (TPU),[8] and polydimethylsiloxane (PDMS).[9–11]

Although single-material flexible sensors demonstrate excellent sensing characteristics, they are prone to interference from external environments. In contrast, sandwich-type flexible sensors can enhance resistance to external interference. The sandwich-type flexible strain sensor, which involves preparing a conductive layer on a flexible substrate and then covering it with a flexible polymer protective layer, can achieve a high sensitivity factor and reduce the shedding of conductive materials.[6,12–14] For instance, Zhou *et al.* utilized the direct ink writing (DIW) process to fabricate composite 2D/3D structures with modified organic silicone oil inks, achieving ultrastretchable printing with a 2000% elongation capacity.[15] Hensleigh *et al.* deposited functional materials into complex structures on the basis of electrostatic attraction, enabling the selective deposition of single metals and various composite materials into specific three-dimensional structures for applications such as tactile sensing, internal wave mapping, and shape self-sensing.[16] Wang *et al.* employed a simple and precisely controlled one-step dual-material 3D printing technology to orderly assemble liquid metal (LM) and elastomer mesh structures into regular solid-liquid two-phase composite materials, resulting in LM/PDMS composites with 180% tensile properties, high conductivity, and excellent electromagnetic shielding properties.[17] Lu *et al.* prepared a dual-function wearable device with electric heating and strain sensing capabilities by combining a crosslinked polyurea elastomer with silver nanowires (AgNWs).[18] However, the aforementioned methods involve multiple processing steps, which complicates the development of new sensors.

To address these challenges, thermoplastic polyurethane (TPU), which can be polymerized under the action of a photoinitiator, has been examined. Previous studies have shown that multiwalled carbon nanotubes–graphene/thermoplastic polyurethane (MWCNT–GN/TPU) flexible sensors exhibit outstanding strain sensing performance.[2] Therefore, in this study, we aim to prepare a sandwich-type strain sensor using a flexible TPU matrix to enhance the performance of the composite material, thereby achieving a high sensitivity coefficient and improved cycle stability. The sensing mechanism relies on the piezo-resistive effect of the MWCNT–GN/TPU composite layer embedded in a photocured sandwich architecture. The resulting sandwich flexible strain sensor boasts a wide operating range (0–105%), a high sensitivity factor [gauge factor (GF) = 2.285], and excellent stability and repeatability, making it suitable for monitoring the motion of flapping wing aircraft. This work is expected to provide a simplified and efficient approach for the development of high-performance flexible strain sensors, addressing the limitations of existing complex processing methods.

2. Materials and Methods

2.1 Materials

The conductive fillers used in this study, carbon nanotubes and graphene, were provided by Shenzhen Yuechuang Evolution Technology Co., Ltd. The carbon nanotubes had a diameter of 10–20 nm, a length of less than 50 μm, and a purity of more than 99.5%. The graphene had a layer thickness of 0.33 nm and a purity exceeding 99.5%. The flexible resin employed was TPU (density: 1.12 g/cm^3), sourced from Dongguan Shenshuo Technology Co., Ltd. The diluent used was IBOMA (purchased from Chengdu Four-city Optoelectronic Materials Co., Ltd.), the dispersant was BYK163 (purchased from Shanghai Kayin Chemical Co., Ltd.), and the photoinitiator was TPO (purchased from Shanghai Kayin Chemical Co., Ltd.). Isopropyl alcohol, used as a cleaning agent, was purchased from Nanjing Xianfeng Nanomaterial Technology Co., Ltd.

2.2 Preparation of conductive composite materials

As suggested by the results of previous studies,[19–21] the combined effect of ultrasonic dispersion and mechanical agitation is beneficial for the dispersion of conductive fillers. A YM-100S3 ultrasonic cleaning machine (Shenzhen Fanao Microelectronics Co., Ltd.) was used in conjunction with an LC-ES-60 digital display agitator (Shanghai Lichen Instrument Technology Co., Ltd.) to prepare the composite slurry at a rotational speed of 1200 rpm, with the entire process conducted in a light-free environment. The ultrasonic treatment and stirring time were set at 30 min. The mass fraction control was maintained at TPU photosensitive resin:IBOMA = 5:1. The mass fraction of the conductive filler was 1.2 wt%, with a mass ratio of MWCNTs:GN = 4:1.

2.3 Fabrication of flexible sensors using a multimaterial DLP system

A self-developed multimaterial photocuring device was employed to achieve the rapid one-piece formation of composite sandwich structures. The formation parameters were as follows: layer thickness of 0.1 mm, three layers of TPU material for the matrix layer, three layers for the intermediate conductive composite layer, and three layers of TPU material for the packaging layer. The exposure time for the TPU matrix material was 1 s with a light intensity of 24 mW/cm^2, while that for the conductive composite material was 90 s with a light intensity of 48 mW/cm^2. After forming the base material, the substrate was lifted and transferred to an isopropyl alcohol cleaning solution for 2 min, then dried by blowing. Subsequently, the substrate was moved to the cylinder containing the conductive composite material to form the conductive structure. After completion, the substrate was transferred back to the cleaning cylinder to remove excess conductive material and again dried. This process was repeated until the desired shape was achieved. Finally, the formed part was placed in a UV box for secondary curing for 5 min to complete the fabrication of the flexible sensor. The multimaterial forming system and the sample are illustrated in Fig. 1.

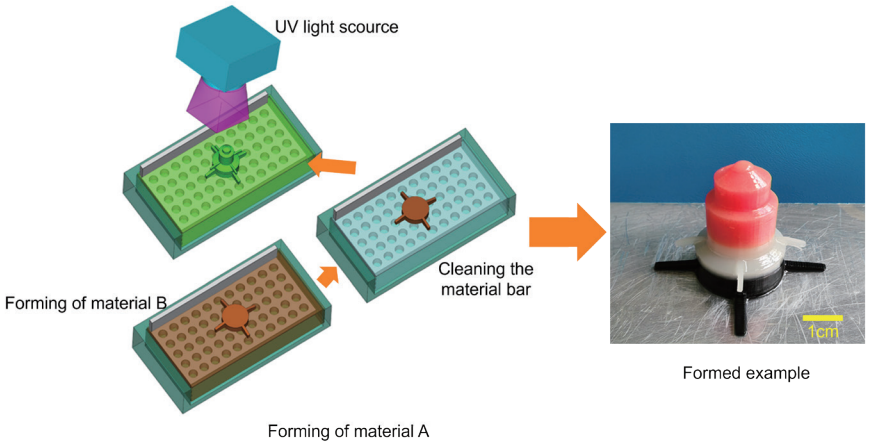

Fig. 1. (Color online) Multimaterial DLP forming system and formed sample.

2.4 Characterization

The morphology of MWCNTs, GN, TPU, and MWCNT–GN/TPU composites was characterized by field emission scanning electron microscopy (Hitachi regulus 8220). The stress–strain curve and mechanical and electrical properties of the strain sensor were measured using a universal material testing machine (China - Sansi Vertical & Vertical -UTM2203) and digital bridge (RK2830, Shenzhen Meiruke Electronic Technology Co., Ltd.). The sample test diagram of the sandwich structure is shown in Fig. 2(a).

The sensor sensitivity factor (GF)[16,22] is calculated as

$$GF = \frac{(R - R_0)/R_0}{\varepsilon} = \frac{\Delta R / R_0}{\varepsilon}, \tag{1}$$

where ε is the strain of the sensor, and R_0, R, and ΔR are the initial resistance, the resistance at deformation ε, and the change in the resistance of the sensor.

To evaluate the adhesion properties of the sandwich material, shear strength tests were conducted. Specifically, the MWCNT–GN/TPU composite was sandwiched between two TPU substrates and cured under a UV lamp for 10 min to ensure proper adhesion. The bonding area for the test was set at 10 × 10 mm^2. Subsequently, tensile tests were performed on the samples at room temperature using a universal testing machine, with the tensile speed maintained at 5 mm/min.

3. Results and Discussion

3.1 Bond strength and mechanical properties

The stable adhesion of the composite material can be attributed to its high cohesion and strong interfacial binding force. This is because the matrix material of the MWCNT–GN/TPU

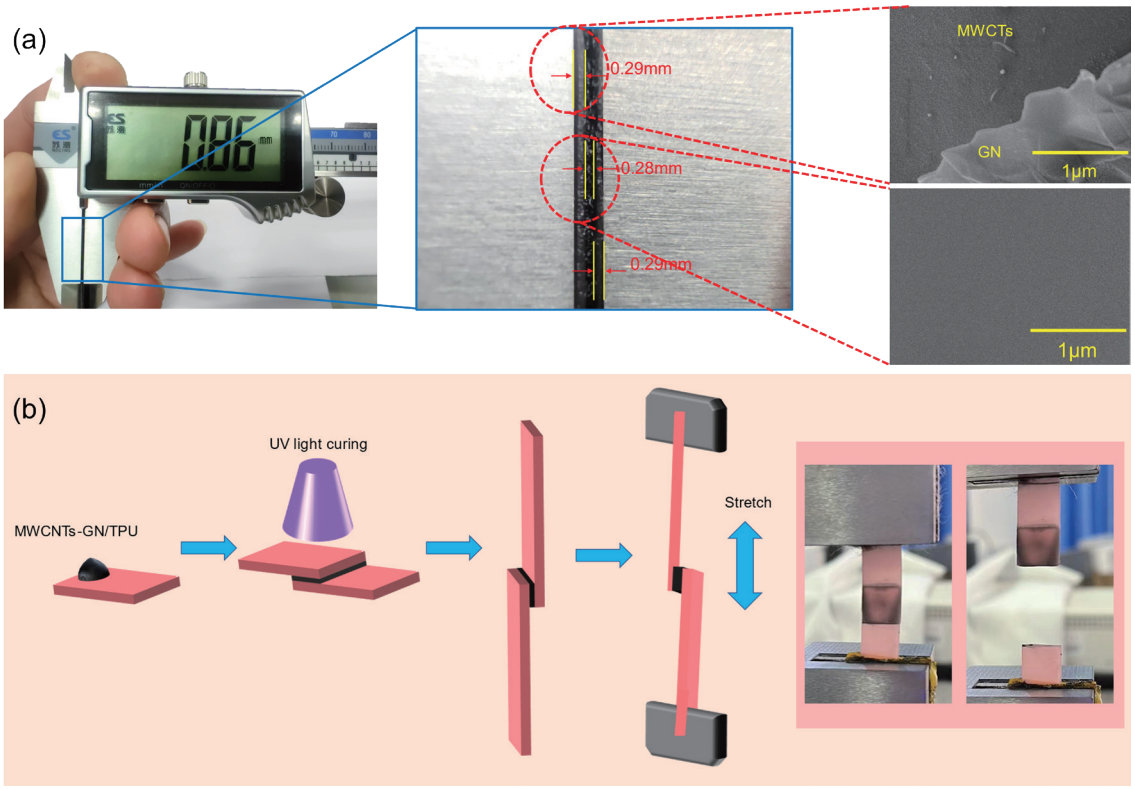

Fig. 2. (Color online) Physical pictures. Photographs of the formed part and the shear strength of the lap joint. (a) Layer thickness measurement and micro-effect of section. (b) Schematic of overlap cut and shear effect.

composite is the same as that of the TPU substrate, which is a TPU-based photosensitive resin. During the photopolymerization process, the identical matrix materials bond together to form an effective adhesive interface. The bonding strength of the sandwich structure was determined by measuring the shear strength [Fig. 2(b)]. The shear fracture result is shown on the right side of Fig. 2(b). The fracture site is the nonadhesive part, indicating that the bonding strength is greater than the fracture strength of the base material.

The mechanical test results are presented in Fig. 3. The Young's modulus of the sandwich structure was measured to be 0.63 MPa, which is 12.5% higher than that of the MWCNT–GN/TPU composite. Additionally, the elongation at the time of breakage of the sandwich structure reached 105%, a 50% increase compared with the 70% elongation at the time of breakage of the MWCNT–GN/TPU composite material. These results demonstrate that the sandwich structure effectively enhances the mechanical properties of the MWCNT–GN/TPU composite, leading to increases in both the elongation at the time of breakage and Young's modulus. This improvement provides the system with a broader strain range, thereby enhancing its mechanical performance and applicability.

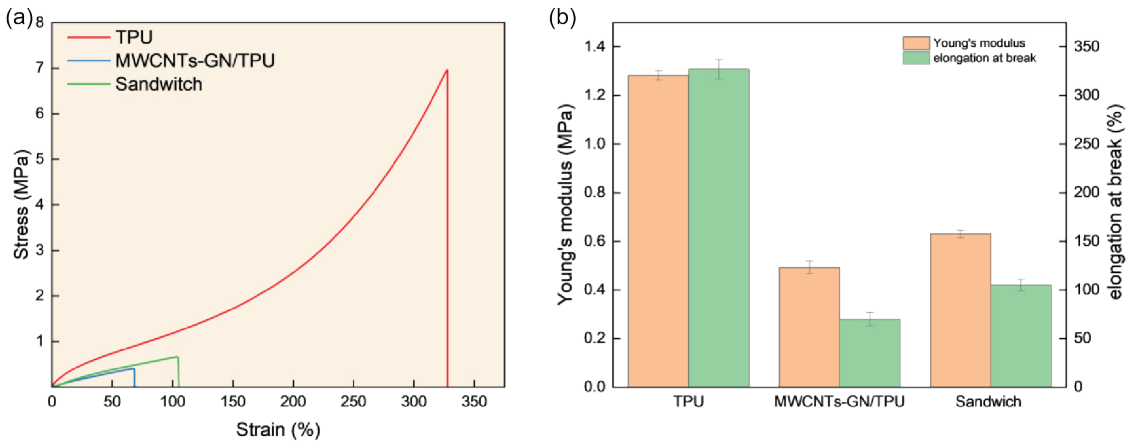

Fig. 3. (Color online) (a) Stress–strain curve and (b) mechanical performance.

3.2 Mechanical hysteresis effect

To compare the mechanical hysteresis of the sandwich structure with that of MWCNTs/TPU composites, the sandwich structure was subjected to cyclic stretching at a tensile speed of 5 mm/min and a strain of 15%. The stress–strain curves were plotted as loading and unloading curves, and the hysteresis of the sandwich structure was characterized using the hysteresis coefficient H_M defined in Eq. 2. The area diagram of the hysteresis curve is shown in Fig. 4(a), while the H_M line diagram, derived from multiple cycle tensile tests, is presented in Fig. 4(b).

The H_M value of the sandwich structure was found to be stable at around 9%, slightly higher than the 8.5% observed for the 1.2-D-TPU composite. This difference may be attributed to the coordination between the high hysteresis effect of the TPU substrate and the 1.2-D-TPU composite material. The conductive filler likely promotes the slip of polymer chains, contributing to the observed hysteresis behavior. However, the presence of a single composite layer within the sandwich structure may delay part of the hysteresis effect. As shown in Fig. 4(b), the H_M value gradually decreases in the first few cycles and stabilizes at 9% by the tenth cycle, exhibiting a trend similar to those of TPU-1.2 and TPU-D-1.2.

The hysteresis coefficient of the sandwich structure is 9%, which is slightly higher than the 8.5% observed for the MWCNT–GN/TPU composite. This suggests that the TPU substrate, with its inherently high hysteresis coefficient, significantly affects the overall hysteresis behavior of the composite structure, leading to an enhancement of the hysteresis phenomenon. The mechanical hysteresis effect coefficient H_M represents the hysteresis phenomenon, and its value is derived from the stress–strain curve during the cyclic tensile process.

$$H_M = \frac{A_L - A_U}{A_L} \tag{2}$$

Here, A_L and A_U represent the areas enclosed by the stress-strain curves and coordinate axes during the tensile and recovery processes, respectively. As shown in Fig. 4(a), the areas of $A_L - A_U$ and A_U are marked as red and blue areas, respectively.

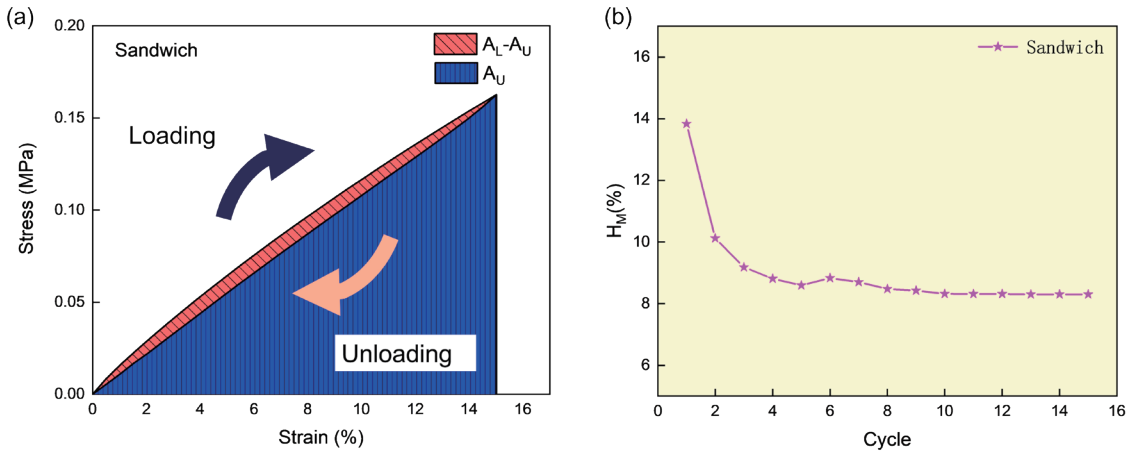

Fig. 4. (Color online) Cyclic stress–strain diagram of sandwich structure: (a) H_M measurement diagram and (b) H_M measurement results.

3.3 Sensing performance

To evaluate the sensing performance of the sandwich structure, its sensitivity was tested, and the results are presented in Fig. 5(a). The sandwich structure exhibited a maximum sensitivity of 5.355 at a large strain of more than 10%. At a strain of 2%, the sensitivity was 1.849, which is likely due to the upper and lower layers of the sandwich structure limiting the strain of the intermediate conductive layer.

To assess the response time of the sandwich structure, the method described above was employed, and the results are shown in Fig. 5(b). The response time was measured to be 340 ms, while the recovery time was 440 ms. These values are slightly higher than those of the MWCNT–GN/TPU composites. This suggests that the sandwich structure delays the response time of the sensor. The higher the hysteresis performance, the faster the response, indicating that the sandwich structure modulates the response time of the composite structure.

3.4 Sensing mechanism

To elucidate the changes in the conductive network within the sandwich structure, the mechanism is illustrated in Fig. 6. In the initial state [Fig. 6(a)], the evenly dispersed MWCNT–GN particles bond together to form a stable and effective conductive pathway. When the sample is stretched [Fig. 6(b)], the conductive fillers elongate with the movement of the TPU molecular chains. This causes the partial disruption of the conductive channels, increasing the distance between the conductive fillers and leading to network disconnection (indicated by the red area). According to the tunneling effect model of resistance[13], increasing the distance between conductive fillers reduces the probability of electron tunneling, thereby increasing the material's resistance.

Simultaneously, stretching separates the MWCNTs from the GN, causing the MWCNTs to re-entangle with each other [Fig. 6(c)] and re-establish a conductive network. This results in

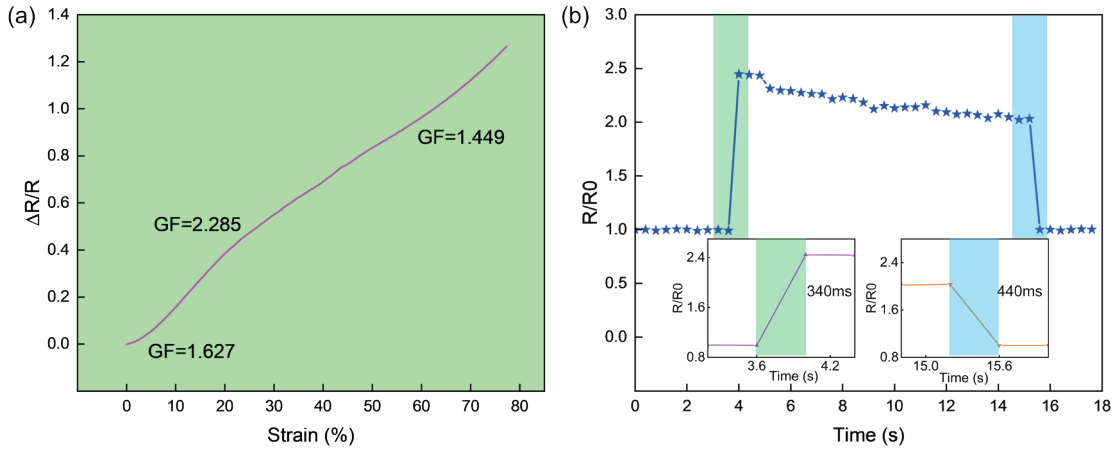

Fig. 5. (Color online) Sensing performance of sandwich structure: (A) results of sensitivity test and (b) measurement results of the response time.

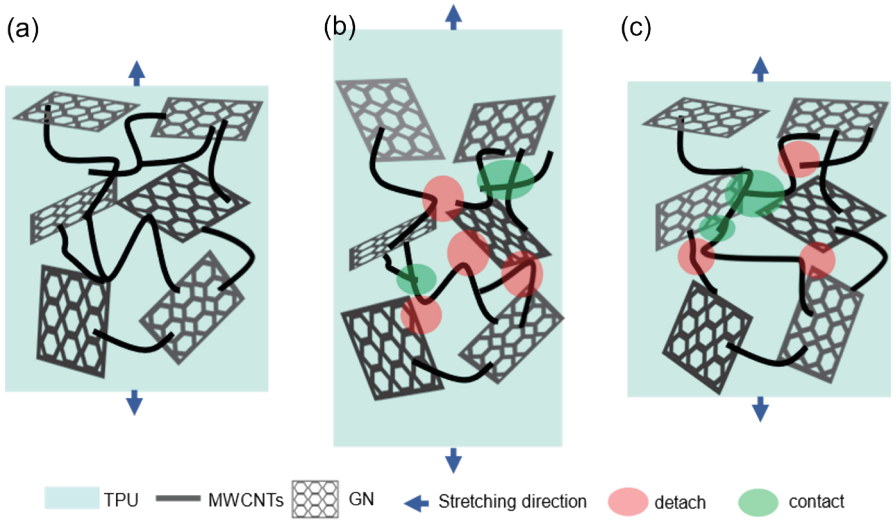

Fig. 6. (Color online) Change mechanism of tensile strain and conductive network of MWCNT–GN/TPU composites under different strains.[21] (a) Conductive network in its initial state; (b) conductive network in a stretched state; (c) conductive network after restoration to its initial state.

resistance fluctuations during the strain recovery process. When the sample returns to its initial position [Fig. 6(c)], part of the conductive network is restored to its original state, leading to a decrease in resistance. However, because of the hysteresis effect of the polymer material and the permanent damage to some conductive channels during stretching, residual resistance remains in the recovery cycle. Eventually, after cyclic stretching, the conductive network stabilizes, and the material exhibits good repeatability and recoverability.

3.5 Potential application

To verify the extensibility and integration capability of the sandwich structure, integrated sandwich ornithine wings were designed and fabricated in accordance with the drawing specifications. The flexible sensor was fabricated by a multi-material DLP system, as illustrated in Fig. 1. The flexible sensor possesses a sandwich architecture wherein both the protective and substrate strata comprise elastomeric TPU resin, while the interposed conductive layer is constituted of MWCNTs-GN/TPU composite. The outer TPU layers were printed with a slice thickness of 0.10 mm for five layers, followed by the conductive layer fabricated at an identical layer thickness (0.10 mm) for nine layers. The fabrication protocol initiated with the photopolymerization of the substrate; the build platform was subsequently elevated, immersed in isopropanol for 2 min to remove unpolymerized resin, dried with compressed air, and transferred into the resin vat containing the MWCNTs-GN/TPU formulation for conductive-layer patterning. Upon completion, the substrate was again rinsed to eliminate residual conductive resin, dried, and over-coated with the protective TPU layer. Finally, the printed construct was subjected to post-curing under UV irradiation for 10 min to enhance polymer conversion and inter-layer adhesion. As shown in Fig. 7, the flexible sensor was conformably attached to the bird wing and interfaced via conductive copper tape to form a series circuit with a precision reference resistor of known resistance. The voltage drop across the sensor was continuously acquired using a digital oscilloscope. Upon aerodynamic deformation, the piezo-resistive response of the sensing film induced a proportional modulation of its electrical resistance, thereby producing a corresponding temporal variation in the measured voltage signal.

Figures 8(a) and 8(b) show two distinct states of the one-piece bird wing. It can be clearly seen that the sandwich flexible sensor occupies a small area of the bird wing, enabling the monitoring of the flight swing of the bird wing. To directly monitor the sensing performance of the flexible sensor on the bird wing sandwich, the sensing performance of the bird wing with a fixed swing frequency was tested. The sandwich structure was attached to the middle part of the wing during the manufacturing process, which can produce large deformations and more intuitively reflect the changes in the wings of the flapping wing aircraft during movement. The

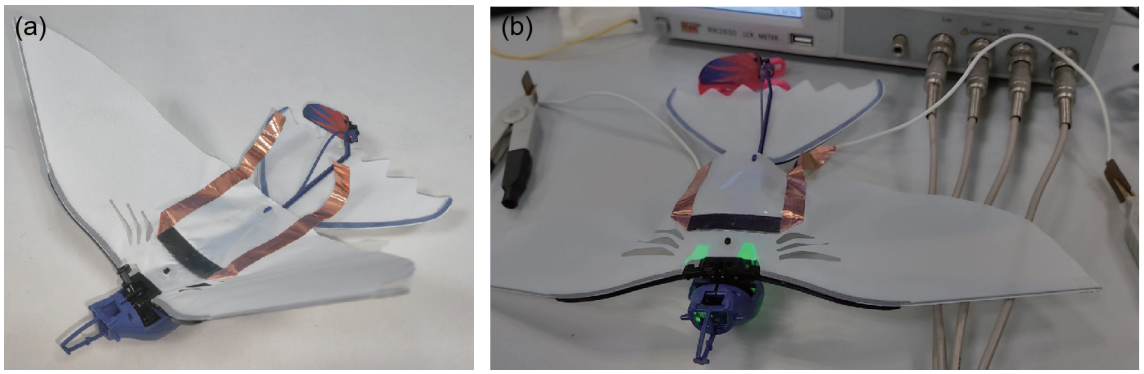

Fig. 7. (Color online) Fabrication of flexible sensor on the bird wing. (a) Flexible sensor on the wing. (b) The voltage of the flexible sensor was monitored.

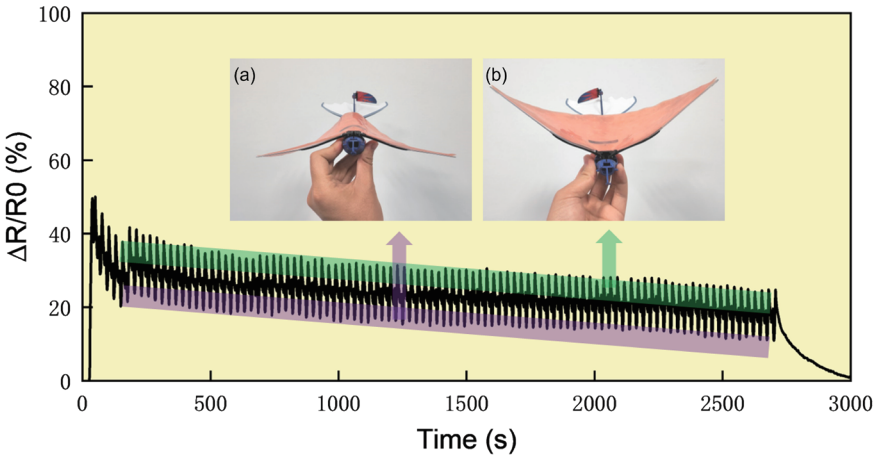

Fig. 8. (Color online) Motion monitoring of ornithopter. (a) Wings are curved. (b) Wings are straightened.

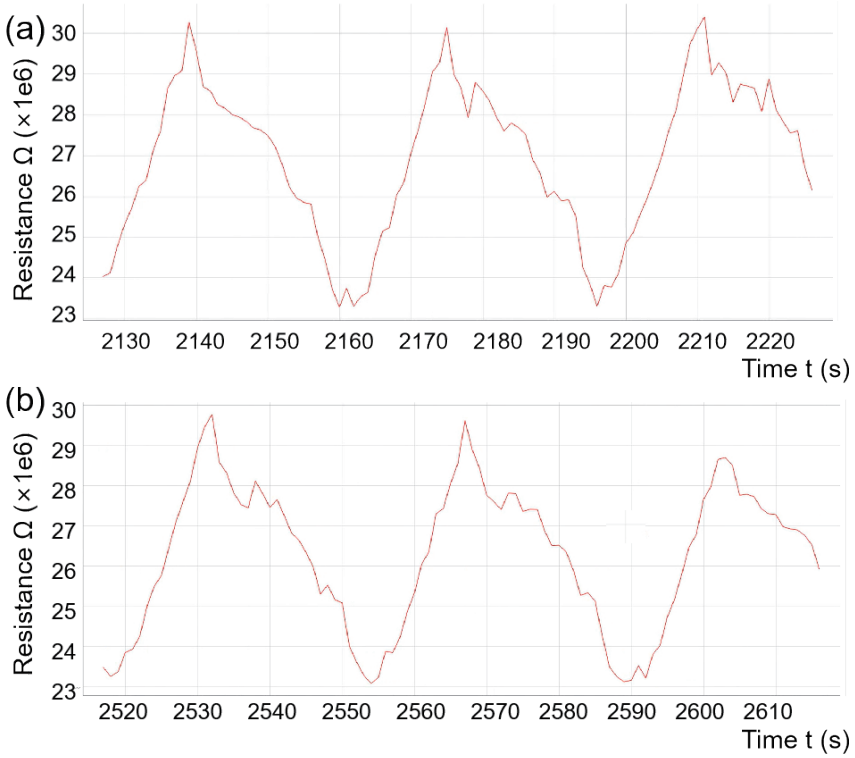

Fig. 9. (Color online) Resistance of the flexible sensor fluctuated in synchrony with the wave of wing. (a) From 2130s to 2220s. (b) From 2520s to 2610s.

test results are shown in Fig. 8, which illustrates the monitoring of multicycle ornithopter flights. Since the wings of the flapping wing aircraft are set to a fixed swing frequency, the resistance change rate curve is approximately straight, as shown in Fig. 9. However, owing to the complex internal structure of conductive polymer materials and the conductive network, the resistance

gradually decreases. For example, the maximum resistance was above 30×10^6 Ω at the time of about 2140 s. However the maximum resistance was below 30×10^6 Ω at the time of about 2530 s. The trend is consistent: when the wings are bent, the sandwich structure is stretched, increasing the resistance, and when it returns to a flat state, the structure is not stretched, resulting in lower resistance. This demonstrates that the method can be effectively used for the integrated preparation of motion monitoring strain sensors for flapping wing aircraft.

4. Conclusions

In this study, a sandwich structure design was employed, utilizing flexible photosensitive resin as both the base and packaging layers, with a 1.2 wt% MWCNT–GN double-packed conductive polymer as the middle layer. The mechanical properties, mechanical hysteresis characteristics, and sensing performance of the sandwich structure were comprehensively evaluated, thereby verifying the feasibility of fabricating sandwich sensors using multiple materials.

The test results revealed that the sandwich structure achieved a strain range of 105%, a significant enhancement compared with the 60% strain range of the 1.2 wt% MWCNT–GN composite. Moreover, the sandwich structure exhibited higher sensitivity, with a maximum value of 5.355. The sandwich structure effectively modulates the hysteresis and mechanical properties of the composite materials, offering a versatile method that is adaptable to various application scenarios.

The flexible sensor fabricated via multimaterial photocuring was successfully applied to monitor the wing movement of an ornithopter, thereby demonstrating the potential application scenarios of this method. Future work may focus on further optimizing the material composition and structure to enhance the sensor's performance and exploring additional applications in fields such as wearable electronics and soft robotics.

Acknowledgments

The authors gratefully acknowledge the financial support from A Project Supported by Jiangsu Provincial Key Research and Development Program (No. BE2019002).

References

1 Y. Shen and Q. Zhu: Sens. Mater. **37** (2025) 2223. https://doi.org/10.18494/SAM5649
2 Q. Lu, Y. Zhou, X. Yin, S. Cao, X. Wang, D. Kong: Research **14** (2021) 9874939. https://doi.org/10.34133/2021/9874939
3 X. Wang, X. Liu, D. W. Schubert: Nanomicro Lett. **13** (2021) 64. https://doi.org/10.1007/s40820-021-00592-9
4 X. Zou, X. Wang, M. Gou, O. Yue, Z. Bai, H. Zhang, and X. Liu: J. Mater. Chem. A Mater. **10** (2022) 14555. https://doi.org/10.1039/D2TA03782C
5 J. Park, N. Jeon, S. Lee, G. Choe, E. Lee, and J. Y. Lee: Chem. Eng. J. **446** (2022) 137344. https://doi.org/10.1016/j.cej.2022.137344
6 T. Xiao, Y. Chen, Q. Li, Y. Gao, L. Pan, and F. Xuan: Adv. Mater. Technol. **8** (2023) 2201376. https://doi.org/10.1002/admt.202201376
7 H. Yang, X. Yao, Z. Zheng, L. Gong, L. Yuan, Y. Yuan, and Y. Liu: Compos. Sci. Technol. **167** (2018) 371. https://doi.org/10.1016/j.compscitech.2018.08.022

8 H. Liu, J. Gao, W. Huang, K. Dai, G. Zheng, C. Liu, C. Shen, X. Yan, J. Guo, and Z. Guo: Nanoscale **8** (2016) 12977. https://doi.org/10.1039/C6NR02216B
9 M. Aakyiir, B. Tanner, P. L. Yap, H. Rastin, T. T. Tung, D. Losic, Q. Meng, and J. Ma: J. Mater. Sci. Technol. **117** (2022) 174. https://doi.org/10.1016/j.jmst.2021.11.048
10 Y. Yang, H. Wang, Y. Hou, S. Nan, Y. Di, Y. Dai, F. Li, J. Zhang: Compos. Sci. Technol. **226** (2022) 109518. https://doi.org/10.1016/j.compscitech.2022.109518
11 C. Zhang, H. Li, A. Huang, Q. Zhang, K. Rui, H. Lin, G. Sun, J. Zhu, H. Peng, and W. Huang: Small **15** (2019) 1805493. https://doi.org/10.1002/smll.201805493
12 X. Fu, M. Ramos, A. M. Al-Jumaily, A. Meshkinzar, and X. Huang: J Mater. Sci. **54** (2019) 2170. https://doi.org/10.1007/s10853-018-2954-4
13 T. Gao, C. Xu, R. Li, R. Zhang, B. Wang, X. Jiang, M. Hu, Y. Bando, D. Kong, P. Dai, and X.-B. Wang: ACS Nano **13** (2019) 11901. https://doi.org/10.1021/acsnano.9b05978
14 D. Lee, M. Seol, G. Motilal, B. Kim, D. Moon, J. Han, and M. Meyyappan: ACS Sens. **5** (2020) 1028. https://doi.org/10.1021/acssensors.9b02544
15 L. Y. Zhou, Q. Gao, J. Z. Fu, Q. Y. Chen, J. P. Zhu, Y. Sun, and Y. He: ACS Appl. Mater. Interfaces **11** (2019) 23573. https://doi.org/10.1021/acsami.9b04873
16 R. Hensleigh, H. Cui, Z. Xu, J. Massman, D. Yao, J. Berrigan, and X. Zheng: Nat. Electron. **3** (2020) 216. https://doi.org/10.1038/s41928-020-0391-2
17 Z. Wang, X. Xia, M. Zhu, X. Zhang, R. Liu, J. Ren, J. Yang, M. Li, J. Jiang, and Y. Liu: Adv. Funct. Mater. (2021) 2108336. https://doi.org/10.1002/adfm.202108336
18 X. Lu, L. Zhang, J. Zhang, C. Wang, and A. Zhang: ACS Appl Mater Interfaces **14** (2022) 41421. https://doi.org/10.1021/acsami.2c11875
19 D. Bai, F. Liu, D. Xie, F. Lv, L. Shen, and Z. Tian: Nanotechnology **34** (2022) 045701. https://doi.org/10.1088/1361-6528/ac9c0b
20 F. Liu, D. Bai, D. Xie, F. Lv, L. Shen, Z. Tian, and J. Zhao: 3D Print Addit. Manuf. (2022) 223. https://doi.org/10.1089/3dp.2022.0223
21 F. Liu, D. Xie, F. Lv, L. Shen, Z. Tian, and J. Zhao: ACS Applied Nano Materials **6** (2023) 4522. https://doi.org/10.1021/acsanm.3c00012
22 X. Cheng, J. Cai, J. Xu, and D. Gong: ACS Appl. Mater. Interfaces **14** (2022) 39230. https://doi.org/10.1021/acsami.2c10226

About the Authors

Deqiao Xie received his B.S., M.S., and Ph.D. degrees from Nanjing University of Aeronautics and Astronautics, China, in 2011, 2014, and 2019, respectively. From 2019 to 2025, he was an assistant professor at Nanjing University of Aeronautics and Astronautics, China. His research interests are in additive manufacturing and sensors. (dqxie@nuaa.edu.cn)

Fuxi Liu received his B.S. degree from Shanxi Agricultural University, China, in 2017, his M.S. degree from Nanjing Agricultural University, China, in 2020, and his Ph.D. degree from Nanjing University of Aeronautics and Astronautics, China, in 2024. From 2024 to 2025, he was an engineer at Beijing Xinghang Electric-Mechanical Equipment Co., Ltd., China. His research interests are in additive manufacturing and sensors. (liufx@nuaa.edu.cn)

Fei Lv received his B.S. and Ph.D. degrees from Nanjing University of Aeronautics and Astronautics, China, in 2014 and 2021, respectively. From 2021 to 2025, he was an assistant professor at Shanghai Institute of Optics and Fine Mechanics, China. His research interests are in additive manufacturing and sensors. (lvfei@siom.ac.cn)